This is a preprint, the final version is subject to change, of the American Mineralogist (MSA)
Cite as Authors (Year) Title. American Mineralogist, in press.
(DOI will not work until issue is live.) DOI: http://dx.doi.org/10.2138/am-2016-5490

Revision 1

Thermodynamics of mixing in an isostructural solid solution: simulation methodologies and application to rutile-cassiterite system

Xin Liu[1, 2] Victor L. Vinograd[3,*] Xiancai Lu[1,*] Egor V. Leonenko[4] Nikolay N. Eremin[4] Rucheng Wang[1] and Björn Winkler[2]

[1]State Key Lab for Mineral Deposits Research, School of Earth Sciences and Engineering, Nanjing University, 210023, Nanjing, China (xinliu.nju@gmail.com; xcljun@nju.edu.cn; rcwang@nju.edu.cn)

[2]Institute of Geosciences, Goethe Universität Frankfurt am Main, 60438, Frankfurt am Main, Germany (b.winkler@kristall.uni-frankfurt.de)

[3]Institute of Energy and Climate Research 6, Forschungszentrum Jülich, 52425, Jülich, Germany (v.vinograd@fz-juelich.de)

[4]Department of crystallography and crystal chemistry, Geological faculty, Moscow State University, 119991, Moscow, Russia (egorleo85@gmail.com; neremin@geol.msu.ru)

Corresponding Author

*E-mail: v.vinograd@fz-juelich.de; xcljun@nju.edu.cn

ABSTRACT

The accuracies of two different approaches to model thermodynamic mixing properties of solid-solutions are explored using the rutile-cassiterite solid solution as an example. Both methods employ an expansion of the configurational enthalpy in terms of pairwise interactions energies. In the first method the partition function is directly computed from the excess energies of all Ti/Sn configurations within a $2 \times 2 \times 4$ supercell. In the second method the free energy of mixing is calculated by a thermodynamic integration of the thermally averaged enthalpies computed with the Monte Carlo method using an $8 \times 12 \times 16$ supercell. The phase relations derived from Monte Carlo simulations agree well with the available experimental data, under the condition that the free energy is corrected for the effect of the excess vibrational entropy. The direct calculation of the partition function provides reasonable phase relations only when the configurational entropy is corrected to be consistent with the ideal mixing in the high-temperature limit. Advantages and drawbacks of the both approaches are discussed. The findings are generally applicable to models of isostructural solid solutions.

Keywords: rutile-cassiterite, solid solution, first principles based calculations, pairwise interactions, Monte Carlo simulations, configurational statistics

1. INTRODUCTION

Rutile-based solid solutions are important as geothermometers. The concentrations of certain trace elements, such as Zr, in rutile serve as indicators of the formation temperatures of its host rock (Cherniak et al., 2007; Watson et al., 2006; Zack et al., 2004a, 2004b). Rutile is also one of the main mineral phases of synroc, the synthetic ceramics proposed for nuclear waste storage (Ringwood et al., 1979a, 1979b; Xu and Wang, 2000; Zhang et al., 2001). Solid solutions with the rutile structure also attract attention as promising candidate materials for photocatalytic and photoelectrochemical energy conversion (Carp et al., 2004; Fujishima and Honda, 1972). The photocatalytic and semiconducting properties of TiO_2 can be modified by doping with various elements. Hence, it is important to understand the thermodynamic properties of this solid solution, and it is well suited as a benchmark to test different modelling approaches aimed at elucidating the properties of isostructural solid solutions.

In this study, a variety of state-of-the-art modelling approaches is applied to predict the extent of the miscibility gap in the rutile-cassitertite solid solution. The main focus is on methodical issues. Thermodynamic functions, which determine the stability of a solid solution, could be computed with methods of statistical mechanics if the energy spectrum of possible configurations of exchangeable atoms is known with sufficient detail. In essence, a model must provide the possibility to evaluate the energy and the Boltzmann weight of any configuration of exchangeable atoms within a supercell of a reasonably large size. However, practically, this detailed configuration-dependent information can be obtained only by computations based on first principles, while a direct sampling of all configurations within a large supercell (i.e. the computation of their energies *ab initio*) is

currently not feasible. In general, two main strategies are used to overcome this problem. One strategy is to directly compute the energies of all configurations, but within a supercell of manageable (smaller) size. The alternative way is to take a sufficiently large supercell, explicitly compute a small set of configurations and employ an interpolation method with which the energy of any configuration can be approximately estimated. For the second alternative there are two further options. Using an interpolation equation one can calculate the energies of all configurations and directly compute the partition function (Becker et al., 2000; Prieto et al., 2000), or apply a Monte Carlo (importance sampling) algorithm to compute approximately the equilibrium enthalpy of mixing and then evaluate the free energy indirectly by a thermodynamic integration (Bosenick et al., 2001; Dove, 2001; Myers, 1998; Reich and Becker, 2006; Warren et al., 2001). One of the aims of this study is to compare the advantages and disadvantages of the last two approaches.

We adopt the following strategy. At first we explicitly compute the excess energies of 20 specially chosen structures within a 2 × 2 × 4 supercell (32 cations) using density functional theory (DFT). Then we employ an interpolation method known as the J-formalism (Becker et al., 2000; Bosenick et al., 2000, 2001; Dove, 2001; Dove et al., 1996, 2000) to compute the pairwise interactions (i.e. the energies of the exchange reactions SnSn + TiTi = 2SnTi) at all distances within a 2 × 2 × 4 supercell of rutile. These energies are then used to derive a generalized Ising-type Hamiltonian of this system, to compute the energies of all possible configurations of Sn and Ti in the 2 × 2 × 4 supercell of rutile and to evaluate the partition function. A correction procedure after Becker et al. (2000) is applied to thermodynamics of mixing to make it consistent with the regular mixing behavior in the high-temperature limit. The same Hamiltonian is then

applied to compute the thermodynamic functions of the system with the aid of the Monte Carlo method by employing an 8 × 12 × 16 supercell. Finally, phase diagrams predicted with the both methods are compared to available experimental data (Garcia and Speidel, 1972; Naidu and Virkar, 1998; Padurow, 1956; Park et al., 1975).

2. STATE-OF-THE-ART MODELLING APPROACHES

2.1. Configuration dependent and configuration independent approaches.

Although all configurations are needed for an adequate model, a variety of configuration-independent approaches exist. At an infinitely high temperature the Boltzmann weights of all configurations are equal and the distribution of exchangeable atoms over the lattice is perfectly random. The mixing behavior of such a solid solution can be assessed with the help of a quasi-random structure (Jiang, 2008; Wei et al., 1990; Zunger et al., 1990). A similar randomization occurs in a diluted solution, although for a different reason. The mixing properties in the dilute limit can be accurately estimated from the excess energy of a supercell structure of a pure (host) phase containing a single substitutional defect of a solute component (Sluiter and Kawazoe, 2003; Vinograd et al., 2013). The solid solution behavior both in the dilute and high-temperature limits can be adequately modeled with the regular or subregular model (Ganguly, 2001). The configuration independent methods provide very useful information on the limiting cases and can serve as good tests for the performance of more sophisticated models.

Configuration dependent approaches can be subdivided into two groups. The first group of methods attempts a direct evaluation of the partition function and the related thermodynamic quantities by sampling *all* configurations within a supercell (Grau-

Crespo et al., 2004, 2007; Liu et al., 2015; Todorov et al., 2004), while other methods compute the energies of only a limited set of configurations and, based on this set, evaluate the energies of the remaining majority of configurations via a parameterized equation (Becker et al., 2000; de Fontaine, 1992, 1994;; Finel, 1994; Laks et al., 1992; Sanchez and de Fontaine, 1978; Sanchez et al., 1984; van de Walle and Ceder, 2002a; Vinograd et al., 2007). Within the second group of methods there are variants, which depend on the approach chosen for the parameterization. One approach, which is now extensively used within materials science, is known as the cluster expansion (de Fontaine, 1994; de Fontaine et al., 1992; Finel, 1994; Laks et al., 1992; Sanchez and de Fontaine, 1978; Sanchez et al., 1984; van de Walle and Asta, 2002; van de Walle and Ceder, 2002a, 2002b). A similar approach, known as the J-formalism became popular in geosciences (Becker et al., 2000; Bosenick et al., 2000; Bosenick et al., 2001; Dove, 2001; Dove et al., 1996, 2000; Ferriss et al., 2010; Jung et al., 2010; Kulik et al., 2010; Reich and Becker, 2006; Renock and Becker, 2011; Vinograd et al., 2007, 2009). Both approaches are briefly outlined below.

2.2. Cluster expansion method and the J-formalism method.

The formalism of the cluster expansion method introduces the occupation variables σ_i, which take values 1 or –1 depending on whether a lattice point i is occupied by A or B atom. A cluster α is defined as a set of points $i,j,k\ldots$, which has a certain fixed location within the lattice and forms a figure of a certain shape (point, pair, triangle, tetrahedron, etc.). The configuration σ_i, σ_j, $\sigma_k\ldots$ of a cluster α can be associated with the cluster function

$$\varphi_\alpha(\sigma) = \sigma_i \sigma_j \sigma_k \ldots \quad (1)$$

It is shown that the cluster functions are orthonormal with respect to the scalar product $\langle \varphi_\alpha(\sigma)\varphi_\beta(\sigma) \rangle$ defined as the normalized sum of products $\varphi_\alpha(\sigma)\varphi_\beta(\sigma)$ over all cluster configurations (de Fontaine, 1994; de Fontaine et al., 1992; Sanchez et al., 1984). From this orthonormality it follows that any function of configuration of a supercell, such as its enthalpy, can be expanded as

$$H(\sigma) = \sum_\alpha J_\alpha \varphi_\alpha(\sigma) \quad (2)$$

where

$$J_\alpha = \left\langle \varphi_\alpha(\sigma) H(\sigma) \right\rangle \quad (3)$$

The macroscopic ensemble averaged enthalpy of a model system (a phase) can be then written as

$$\left\langle H \right\rangle = \sum_\alpha J_\alpha \xi_\alpha \quad (4)$$

where ξ_α is the ensemble averaged cluster function, which is called the correlation function of the cluster α. The practical advantage of Eq. 4 consists in its rapid conversion with respect to an addition of terms corresponding to clusters of larger size. This mathematically rigorous expansion method includes a rigorous definition of the effective cluster interactions via Eq. 3. From this definition, the effective pair cluster interaction energy takes the form

$$J_{pair(n)} = \frac{1}{4}\left(\left\langle H_{\mathrm{AA}(n)} \right\rangle + \left\langle H_{\mathrm{BB}(n)} \right\rangle - \left\langle H_{\mathrm{AB}(n)} \right\rangle - \left\langle H_{\mathrm{BA}(n)} \right\rangle \right) \quad (5)$$

where $H_{ij(n)}$ is the energy of a supercell with an *ij* pair in a fixed *n*-th location within a supercell at the fixed distance, d_n, between the atoms *i* and *j*, while the average is taken

159 over all possible configurations of the other atoms in the supercell. An important property
160 of the cluster expansion is that all correlation functions of a completely disordered
161 (A,B)*R* solid solution with the composition of x_A= 0.5 are equal to zero. Thus, when all
162 quantities are measured relative to a mechanical mixture of end-members, it appears
163 necessary to introduce a constant, J_0, the so-called zero cluster interaction, and postulate
164 that the correlation function of the zero cluster is equal to 1. J_0 is equal to the enthalpy of
165 mixing of a completely disordered (uncorrelated) solid solution with the composition of
166 x_A= 0.5. This completely disordered state ($J_0 \neq 0$, $\xi_0 = 1$, $\xi_n = 0$, $n > 0$) represents the
167 central point of the cluster expansion of Sanchez et al. (1984) The terms of the cluster
168 expansion with $n > 0$ describe deviations of the enthalpy of a real solid solution from this
169 reference state. In this sense the end-members and ordered intermediate compounds are
170 treated on equal grounds as different examples of extremely correlated states.
171 The J-formalism (Bosenick et al., 2000, 2001; Dove, 1999, 2001; Dove et al., 1996, 2000;
172 Palin et al., 2001; Warren et al., 2001; Will, 1998) is often understood as a restricted form
173 of the cluster expansion, in which the cluster size is limited to a pair of points. However,
174 this is not exactly true. Aside from being limited to pairs, the J-formalism assumes also a
175 different reference state. The reference state of the J-expansion is not a disordered state
176 with x_A = 0.5, but rather a mechanical mixture of the end-members A*R* and B*R*.
177 Consequently, a constant, J_0, term is not required in the J-formalism. The basic idea of
178 the J-formalism is that any deviation of the enthalpy of a solid solution from the enthalpy
179 of a mechanical mixture is correlated with the production of pairs of AB type. Therefore,
180 in the J-expansion the J terms are coupled not to correlation functions, but to probabilities
181 of AB pairs. The pairwise interaction is thus defined as a contribution to the excess

enthalpy of a solid solution due to the formation of one AB pair (or one mole of AB pairs). As the production of two AB pairs is necessarily related to an annihilation of a couple of AA and BB pairs, the pairwise interaction is defined as

$$J_{(n)} = 2\left\langle H_{\mathrm{AB}(n)}\right\rangle - \left\langle H_{\mathrm{AA}(n)}\right\rangle - \left\langle H_{\mathrm{BB}(n)}\right\rangle \quad (6)$$

where the quantities in brackets have the same meaning as in Eq. 5. The $J_{(n)}$ terms are thus proportional to the effective pair interactions in the cluster expansion (de Fontaine, 1994; de Fontaine et al., 1992), but have a different sign. Similarly to the cluster expansion, the J-formalism can include clusters, which are larger than pairs. Indeed, the probabilities of AAB, ABB, AAAB, AABB, ABAB and ABBB are also constrained to be identically zero in the state of a mechanical mixture and thus the relevant ternary and quaternary terms could be easily included in the J-expansion. This is not done because of practical reasons. Ternary or higher-order interactions are usually much weaker than the pair interactions. The reason for the complete exclusion of the higher order interactions in applications to minerals comes from the observation that in oxides, silicates, carbonates or phosphates the exchangeable atoms (typically represented by cations) never appear in close contact with each other, as they do in alloys. In minerals the cations are usually separated by anion groups that remain inert to the mixing. Strong specific ternary or quaternary interactions, which could appear due to an association of several cations in a close proximity of each other, become less likely. The enthalpy of mixing for a configuration *i* is written as

$$H_i = 1/2\sum_{n=1}^{N} J_n Z_n P_{\mathrm{AB}(n)} \quad (7)$$

where Z_n is the coordination number within a sublattice occupied by neighbors of the order *n*. The order of neighbors, *n*, usually corresponds to the distance between the atoms.

205

206 **2.3. Determination of the *J*s.**

207 The methods for the evaluation of the *J* terms are similar in the cluster expansion and in
208 the J-formalism. The cluster inversion (Connolly and Williams, 1983; de Fontaine, 1994;
209 de Fontaine et al., 1992) procedure is based on the assumption that the quantities defined
210 by Eq. 5 are relatively insensitive to the number and types of configurations included in
211 the summation, such that they could be considered as configuration and composition
212 independent constants. Thus, one is allowed to expand the energies of several compounds
213 differing in symmetry and composition using the same set of the cluster terms by
214 assuming that the effective interactions are the same in all compounds. In alloys these
215 compounds are usually selected based on experimentally observed ordered phases. In this
216 way one obtains a set of equations, which can be solved for the effective interactions. The
217 J-formalism is typically applied to low-symmetry lattices, where the selection of ordered
218 compounds is difficult. Therefore, the anchor structures/configurations are often selected
219 at random within a supercell of a certain shape. The averaged normalized numbers of AB
220 pairs in all these structures are counted at all distances and the system of equations of the
221 type of Eq. 7 is solved for the J_n with the least-squares method (Becker et al., 2000;
222 Ferriss et al., 2010; Reich and Becker, 2006; Renock and Becker, 2011; Vinograd et al.,
223 2006, 2007).
224 An alternative way of evaluation of the *J*s is to consider three supercells with the
225 specified AA, BB and AB configurations and with the rest atoms in the same
226 configurations and directly apply Eq. 5 or 6. Keeping the AA, BB and AB arrangement
227 fixed, the rest atoms are permuted and the calculation is repeated. The *J* value can be

228 computed as the averaged energy obtained by a summation over a limited set of these
229 configurations. It has been shown that this procedure can give converged values by
230 averaging over about 20-50 randomly chosen configurations with fixed AA, BB and AB
231 arrangements (de Fontaine et al., 1992; Wolverton et al., 1991). The double defect
232 method (DDM) (Asato et al., 2001; Hoshino et al., 1993, 1996; Vinograd et al., 2009;
233 Vinograd and Winkler, 2010) is a variant of this approach, where only two unique
234 configurations are considered, namely, the configurations with "all A" and with "all B".
235 In the "all A" case the AB, AA and BB pairs are inserted in the supercell of the A*R* end-
236 member. As in this case the A atoms of the pair cluster are indistinguishable from the rest
237 A atoms of the host supercell, Eq. 5 or 6 effectively requires the computation of the
238 energy difference between two supercells with a single defect B, a supercell of the pure
239 end-member A*R* and a supercell with a double BB defect with the B atoms fixed at a
240 certain distance from each other. When the energies of all structures are counted relative
241 to the mechanical mixture of A*R* and B*R*, end-members, the recipe can be further
242 simplified as follows

243 $$J_{\mathrm{A}(n)} = (2\Delta H_{\mathrm{B}} - \Delta H_{\mathrm{BB}})/D_n \qquad (8)$$

244 where ΔH_{B} and ΔH_{BB} are the excess enthalpies of the supercells with a single, B, or a
245 double, BB, defect, respectively, and D_n is the degeneracy factor, which counts the
246 multiplicity of BB pairs due to the use of periodic boundary conditions in the model
247 calculations. An analogous equation is written for the "all B" case

248 $$J_{\mathrm{B}(n)} = (2\Delta H_{\mathrm{A}} - \Delta H_{\mathrm{AA}})/D_n \qquad (9)$$

249 As the DDM naturally provides two sets of the J_n values, it is convenient to model
250 intermediate compositions by a linear mixing of $J_{\mathrm{A}(n)}$ and $J_{\mathrm{B}(n)}$

$$J_n = x_{\mathrm{A}} J_{\mathrm{A}(n)} + x_{\mathrm{B}} J_{\mathrm{B}(n)} \quad (10)$$

The composition dependence appears to be an important advantage of the DDM over the standard J-formalism. The method also allows to significantly reduce the number of supercell structures to be computed. Effectively, the determination of a single pairwise interaction requires the computation of a single supercell structure with a paired defect.

2.4. Calculation of thermodynamic quantities via direct sampling of all configurations.

Here we assume that the total excess Gibbs free energy can be split into the configurational and vibrational parts, while the vibrational free energy is insensitive to configuration, but depends on the composition. This simplification can be justified when the excess vibrational free energy is small and its effect is expected to be significant only at high temperatures. This effect is modeled here with the aid of quasi-random structures. The configurational part is modeled with the J-formalism. First the J_n values are substituted into Eq. 7 to compute the energies of all possible configurations of a given supercell. When the energies of all configurations are known, the free energy per 1 mole of exchangeable atoms at a temperature T (K) can be computed as

$$G = -(1/p)RT\ln Z \quad (11)$$

where p is the number of exchangeable sites within the supercell, R=8.314 J/K/mol is the gas constant and

$$Z = \sum_i \exp\left(-H_i/(RT)\right) \quad (12)$$

is the partition function. The summation is often taken only over symmetry non-equivalent configurations, which could be enumerated with available programs, for

example, SOD (Site Occupancy Disorder) (Grau-Crespo et al., 2004, 2007). Each exponential term is then counted with its multiplicity. The ensemble average enthalpy is computed as

$$H = \frac{1}{pZ}\sum_i \exp\left(-H_i/(RT)\right)H_i \quad (13)$$

The configurational entropy is then calculated as

$$S = \frac{H - G}{T} \quad (14)$$

It should be noted that the entropy computed with this approach would deviate from the ideal mixing entropy even in the high-temperature limit. Due to the limited size of the supercell, the maximum entropy is given by

$$S_{\max} = (R/p)\ln\binom{p}{k} \quad (15)$$

where k is the number of atoms of type B. For a small cell this value could be significantly smaller than the entropy of ideal mixing

$$S_{\text{ideal}} = -R(x_{\text{A}}\ln x_{\text{A}} + x_{\text{B}}\ln x_{\text{B}}) \quad (16)$$

For example, for a cell containing 24 sites, the maximum entropy computed with Eq. 16 is about 11% smaller than the ideal mixing value. Becker et al. (2000) suggested an elegant procedure, which corrects for this drawback. In their procedure, the manifold of configurations is viewed as the probability vs. energy distribution scaled by the total number of configurations. The sum in Eq. 12 is then substituted with an integral over this distribution, while the number of configurations is taken out of the integral sign. The Gibbs free energy can be then written as

$$G = -\frac{RT}{p}\ln\binom{p}{k} - \frac{RT}{p}\ln\frac{\int_0^\infty \exp(-H/(RT))p(H)dH}{\int_0^\infty p(H)dH} \quad (17)$$

The correction consists in the replacement of the first term with the negative of the ideal entropy times T

$$G = RT(x_A \ln x_A + x_B \ln x_B) - \frac{RT}{p}\ln\frac{\int_0^\infty \exp(-H/(RT))p(H)dH}{\int_0^\infty p(H)dH} \quad (18)$$

.

Eq. 18 correctly predicts the regular mixing behavior only in the high-temperature limit. The correction does not remove all drawbacks of a small-supercell model. An important problem of such a model is its inability to represent a proper relationship between the frequencies of ordered and disordered configurations. Indeed, in a small supercell the ratio of disordered to ordered configurations is inevitably underestimated. Consequently, in a small supercell short-range order has a weaker effect on the free energy of the disordered state. As the free energy of the disordered phase cannot be effectively decreased on cooling by SRO effects, it becomes less stable relative to an ordered phase (or to the mixture of end-members) at a rather high temperature. The order/disorder transition temperature is thus overestimated.

2.5. Calculation of thermodynamic quantities via Monte Carlo simulations.

The obvious remedy for the former method is to enlarge the supercell size. However, the alternative large-cell models have to deal with the problem of an intolerable increase in the number of configurations. There have been attempts to deal with the problem of "configurational explosion" by limiting the number of sampled configurations. A feasible approach is to select a subset of a few hundred of configurations by sampling them at

315 random (Allan et al., 2001, 2006; Purton et al., 2006; Todorov et al., 2004). This
316 approach, however, often predicts free energies, which only marginally deviate from the
317 regular mixing model. Configurations sampled in this way typically represent the largest
318 pool of highly probable high-energy configurations. These configurations have similar
319 (high) energies and similar Boltzmann weights. Therefore, configurational entropy
320 computed from such a reduced set appears to be close to that of the ideal mixing model,
321 while the configurational enthalpy closely follows the Margules model. A similar result
322 can be more easily obtained with a quasi-random structure. Recently, D'Arco et al.
323 (2013) offered a modified algorithm, in which the subset of states is obtained by random
324 sampling over classes of symmetry independent configurations. The applicability of this
325 algorithm to large supercells and thus for accurate computation of phase diagrams is still
326 to be demonstrated.
327 The importance sampling via a Monte Carlo algorithm (Metropolis et al., 1953) can be
328 conveniently applied to much larger supercells than those typically employed in direct
329 methods. The average enthalpy of the sampled set energy is correctly shifted to a lower
330 value, which reflects higher weights of low energy configurations at a finite temperature.
331 The configurational enthalpy computed with a supercell containing few thousands of
332 exchangeable sites is essentially correct. However, the entropy value computed from such
333 a limited subset would still be close to that of the ideal mixing model as the energies of
334 the converged set of configurations fluctuate only slightly from this average (although
335 correct) value of the enthalpy. The evaluation of the correct entropy value requires
336 computation of the partition function or the Gibbs free energy. While a direct evaluation
337 of the former is difficult, the equilibrium Gibbs free energy can be computed relatively

easily using thermodynamic relations under the assumption that the average enthalpy computed by the Monte Carlo method is correct. The relationship between the free energy and the enthalpy is given by the integral (Dove, 2001; Myers, 1998; Warren et al., 2001):

$$G = RT(x_A \ln x_A + x_B \ln x_B) + \langle H \rangle_0 + \int_0^{\lambda} \langle H \rangle_{\lambda} d\lambda \qquad (19)$$

where λ, $0 < \lambda < 1$, is an artificial variable used to scale the magnitude of the effective pairwise interactions down, and $\langle H \rangle_\lambda$ is the enthalpy averaged over an ensemble, in which the probability distribution of all configurations corresponds to the effective pairwise interactions scaled by λ value. In the application to the J-formalism, the evaluation of $\langle H \rangle_\lambda$ requires a Monte Carlo simulation of a system, in which the pairwise interactions are scaled by λ. It should be remembered the converged enthalpies resulting from the simulation should be rescaled back (i.e. divided by the same λ value). The first two terms in Eq. 19 correspond to the Gibbs free energy of the solid solution in the state of a complete disorder, which is known theoretically, while the integral describes the deviation of the real free energy at the given temperature from the reference state.

The power of the integration method is based on the ability of the Metropolis algorithm to arrive at the correct average (equilibrium) energy without the need of sampling all possible states. Consequently, the method can be applied to a sufficiently large cell, such that the averages are indistinguishable from the case of the thermodynamic limit. When the Markov chain of Monte Carlo stated converges to the Boltzmann distribution, each symmetry independent configuration occurs with the correct probability. Thus the correct average enthalpy can be computed by sampling a sufficient number of successive states. For example, the computation of an enthalpy value at a high temperature does not require

sampling of the ground state configuration. The probability of this configuration at a high temperature is vanishingly low and its contribution to the average energy is similarly small. This configuration, however, becomes very important at a low temperature, thus, as noted, for example, by d'Arco et al., 2013, there is a possibility that such a rare configuration could be missed in a simulation. The art of the simulation thus consists in gradually decreasing the temperature and in restarting from previously equilibrated configurations. Our experience suggests that the finding of the correct ground state is always possible in supercells containing less than about 4000 sites. There are different means that help to ensure that the correct state is found. One possibility is to check that the same final enthalpy is achieved in runs that start from different initial configurations. In the present case, where the ground state is represented by a miscibility gap, there appears a possibility to observe fine features within the isotherm shape, that are related to changes in the form of the interface between the two phases. Observing these fine features, in fact, means that true equilibration has been achieved.

3. COMPUTATIONAL DETAILS

The pairwise interactions were computed from the excess energies of $2 \times 2 \times 4$ supercells of rutile structure (TiO_2 or SnO_2) containing substitutional defects of Ti and Ti-Ti in the case SnO_2 being the host or Sn and Sn-Sn defects in the case of TiO_2. The paired defects were placed at 10 different distances in the range of 2-9 Å. The size of the supercell was chosen such that the computed interaction between the pair of defects placed at the longest distance practically vanishes. The total energies of the single- and double-defect structures were calculated with density functional theory in the Wu-Cohen (WC GGA)

384 approximation (Wu and Cohen, 2006) using the "on-the-fly" ultrasoft pseudopotentials
385 integrated in the CASTEP distribution, version 7.03 (Clark et al., 2005; Segall et al.,
386 2002). The plane wave expansion cutoff was 900 eV. The k-space was sampled using a 3
387 × 3 × 3 Monkhorst-Pack grid.
388 Although Eqs. 8 and 9 could be directly applied for computing the pairwise interactions,
389 the resulting values of the *J*s often lack self-consistency (Vinograd et al., 2009; Vinograd
390 and Winkler, 2010). The requirement of self-consistency is based on the observation that
391 although the *J*s are directly determined by the excess energies of the defect structures via
392 Eqs. 8 and 9, the excess energies themselves are functions of the *J*s via Eq. 7. This
393 implies that the excess energies of the single- and double-defect structures should be
394 exactly reproduced via Eq. 7. This requirement is often violated due to slight
395 inaccuracies in the computed excess energies of the single- and double-defect structures
396 or due to the presence of higher-order interactions. The self-consistency can be restored
397 by a slight variation in the excess energies of the single defect structures, which occur in
398 Eqs. 8 and 9. Practically, small parameters δ_1 and δ_2 are added to ΔH_A and ΔH_B
399 respectively, and their values are varied until the excess energies of the double-defect
400 structures are reproduced exactly via Eqs. 7-10.
401 Monte Carlo simulations were performed with an 8 × 12 × 16 supercell containing 3072
402 exchangeable atoms. The size of the supercell was chosen based on previous experience.
403 It can be shown that the critical temperature in the well-studied two-dimensional square
404 lattice with nearest-neighbor interactions [Onsager, 1944] can be reproduced with a
405 relative accuracy of better than 5% using supercell containing about 2500 lattice sites.
406 However, to our experience, a significant increase over this number could cause

difficulties in finding correct ground states. Our previous experience (Jung at al., 2010; Vinograd et al., 2007) with various three-dimensional lattices suggest that the optimal supercell should contain about 3000 or 4000 sites. The average enthalpy at a given composition and temperature was calculated assuming a canonical ensemble using the Metropolis algorithm (Metropolis et al., 1953). At each simulation step a pair of different atoms was chosen at random and the swap was attempted. The swap was either accepted or rejected depending on the enthalpy change due to the swap, ΔH. A new configuration was accepted for $\Delta H \leq 0$ or with the probability of $\exp(-\Delta H/k_B T)$ for $\Delta H > 0$. The distribution was assumed to converge to the Boltzmann probability distribution after 2×10^7 steps. The next 2×10^7 steps were used to calculate the averages. The simulations were performed with the J values computed with Eq. 10, the temperature was varied between 600 K and 2500 K with an interval of 100 K and the composition was varied with a step of 0.03125. For each temperature and composition the calculations were repeated 26 times at different λ values, where λ was varied from 0 to 1 with a step of 0.04.

The excess vibrational entropy of mixing was calculated with an empirical force-field model. The interatomic potentials were fitted to the structure data of rutile (Swope et al., 1995), brukite (Baur, 1961), anatase (Horn et al., 1972) and cassiterite (Baur, 1956), and to the elastic stiffness tensors of rutile and cassiterite (Ahrens, 1995). The parameters are listed in Table 1. The unit-cell parameters and the elastic stiffness constants of rutile and cassiterite calculated with these potentials are given in Table 2. The vibrational free energies of the end-member structures and of the quasi-random structures (QRS) were computed with the GULP program (Gale, 1997, 2005; Gale and Rohl, 2003). using the

zero static internal stress approximation (ZSISA) (Allan et al., 1996). The force-field model was tested against the *ab initio* data (Sikora, 2005) for pure rutile. The thermodynamic properties (entropy and heat capacity at constant volume) of rutile deviate over the temperature interval of 300-2500 K by less than 3% from the DFT results. The effective excess vibrational entropy of the QRS was computed as the negative of the excess vibrational free energy divided by T. The entropies were averaged in the temperature range of 1473-1773 K and fitted to the equation

$$S_{\text{vib}} = x_{\text{A}} x_{\text{B}} (x_{\text{A}} W_{12}^{s} + x_{\text{B}} W_{21}^{s}) \quad (20)$$

where x_{A} and x_{B} are mole fractions of rutile and cassiterite in the solid solution, respectively. The contribution of the excess vibrational free energy to the free energy of mixing was computed as $-TS_{\text{vib}}$.

The quasi-random structures (x_{Sn}=0.25, x_{Sn}=0.5 and x_{Sn}=0.75) were found by a direct search among all possible configurations within a 2 × 2 × 4 supercell. During the search the frequencies of Ti-Sn pairs at 10 different distances were compared to their theoretical probabilities. The misfit function was defined as the total squared difference between the actual and the theoretical frequencies. Structures (configurations) corresponding to the minimum misfit were selected.

4. RESULTS

4.1. Quasi-random and single-defect structures.

The excess enthalpies of the structures with single defects (0.3899 eV per supercell for Ti in SnO_2 and 0.4056 eV per supercell for Sn in TiO_2) provide constraints for the subregular model of the enthalpy of mixing

453 $$H_{\infty} = x_{\mathrm{A}} x_{\mathrm{B}} (x_{\mathrm{A}} W_{12}^{h} + x_{\mathrm{B}} W_{21}^{h}) \qquad (21)$$

454 The Margules parameters W_{12}^{h} = 39.13 kJ/mol and W_{21}^{h} = 37.62 kJ/mol are
455 straightforwardly computed by applying the conversion factor of 96.485 kJ/mol/eV to the
456 excess enthalpies of the single-defect structures (Vinograd et al., 2013). The slightly
457 larger value of W_{12} reflects the increased difficulty of inserting a larger cation (Sn) into a
458 structure with a smaller mole volume (TiO_2). The excess energies of the quasi-random
459 structures are similar to that obtained from Eq. 21 (Fig. 1), because the structures with
460 single defects comply with the criteria of QRS. This consistency between the excess
461 enthalpies confirms the good quality of the QRSs. These structures can hence be used for
462 modelling the properties of a completely disordered solution. The same conclusion
463 applies to the single-defect structures as well.

464 The regular model of the enthalpy of mixing, (W_{12}^{h} + W_{21}^{h})/2 = 38.4 kJ/mol,
465 straightforwardly predicts the critical temperature of the phase separation at x_{Sn} = 0.5 as
466 $T_c = W/2R$, i.e. 2309 K (Glynn, 2000; Park et al., 1975; Urusov et al., 1996). This value
467 significantly overestimates the experimental temperatures of 1703±5 K (Park et al., 1975)
468 and 1689 K (Naidu and Virkar, 1998), showing that the regular (or subregular) model is
469 not adequate for this system. Within the regular model description this temperature could
470 be brought into correspondence with the experiment only under the assumption that the
471 excess vibrational entropy constitutes about 25% of the configurational entropy. As we
472 will show below, the vibrational contribution appears to be much smaller. A more
473 adequate model requires consideration of short-range order (SRO) effects. Indeed, SRO
474 effects allow a significant stabilization of the disordered phase, which leads to a decrease
475 in the transition temperature. SRO is primarily driven by pairwise interaction energies.

476

477 **4.2. Parwise interactions.**

478 Fluctuations in excess energies of the paired defects Ti-Ti in rutile and Sn-Sn in
479 cassiterite reflect variations in the defect-defect interaction at different distances (Table
480 3). As these interactions should decrease with the increase of the distance between the
481 defects, the excess energies of the defect-defect structures are expected to converge to
482 twice the excess energy of the single-defect structure. Simultaneously, the effective
483 interactions should converge to zero value (Fig. 2). This behavior is indeed observed.
484 The small final values of the δ_1 and δ_2 parameters, -0.000081 and 0.000011 eV,
485 respectively, show that the computed excess energies of the single- and double-defect
486 structures are very close to internal consistency. The small deviations could be caused by
487 the presence of interactions of higher order although these interactions must be very
488 weak. The *J* values determined from this fit are listed in Table 3. Fast convergence of the
489 *J* values as a function of interatomic separation (Fig. 2) implies the applicability of these
490 parameters for the calculation of the excess enthalpies using much larger supercell.

491

492 **4.3. Direct method with a 2 × 2 × 4 supercell.**

493 All configurations were permuted with a self-written C program and their excess energies
494 were evaluated via Eq. 7. Figure 3a, 4a and 5a show the results of the excess enthalpy,
495 the free energy and the configurational entropy computed via Eqs. 13, 11 and 14,
496 respectively.
497 The wavy shapes of the low temperature isotherms reflect ordering, which would have
498 occurred in the system if the phase separation were forbidden (Fig. 3a, 5a,b). The minima

correspond to structures with alternating layers fully filled with Sn or Ti atoms, which are parallel to (100) or (010). Figure 4a shows that the phase separation at intermediate compositions occurs at about 2000 K. Thus the ordered states are never stable with respect to a mixture of Ti- and Sn-rich phases. Figure 5a shows also that at high temperatures the configurational entropy converges to values, which are significantly smaller relative to the ideal mixing model. This drawback of the 2 × 2 × 4 model leads to a significant overestimation of the free energy of the disordered phase at high temperatures and, consequently, to an overestimation of the solvus temperature.

4.4. Direct method with a 2 × 2 × 4 supercell and with the entropy correction.

In the method of Becker et al. (2000) the free energy is evaluated via Eq. 18. This leads to a significantly more negative free energy of mixing at high temperatures and, consequently, to a lower temperature of the solvus closure (Fig. 4b). The corrected configurational entropy becomes consistent with the high-temperature limit of the ideal mixing model (Fig. 5b). However, the low-temperature entropy isotherms shift to larger values.

4.5. Monte Carlo simulation using an 8 × 12 × 16 supercell.

The enthalpy of mixing, the free energy and the configurational entropy resulting of these simulations are given in Figure 3b, 4c and 5c, respectively. The shapes of low-temperature isotherms differ significantly from those computed with the direct method. This is the consequence of the phase separation (Fig. 6), which occurred during the Monte Carlo simulation runs. In contrast, in the direct method the phase separation does

not occur within the small supercells and thus does not affect the shape of the isotherms. The direct method includes configurations, which formally could be interpreted to represent phase separation. However, due to the relatively large interface energy, the energies of these configurations appear to be higher than the corresponding ordered structures and thus do not contribute much to the shapes of low-temperature isotherms.

4.6. Vibrational entropy correction and the phase diagram.

Figures 3-5 correspond to the model, which is based on static energies only. However, each configuration is also characterized by its own vibrational entropy and free energy. Our calculations based on quasi-random structures suggest that the vibrational entropy adds about 10% to the total entropy of mixing at high temperatures and intermediate compositions (Fig. 7). The curve of the vibrational entropy is asymmetric (W_{12}^{s}=1.66, W_{21}^{s}=3.02 J/K/mol). The sense of asymmetry is similar to that of the enthalpy of mixing.

The phase diagram of rutile-cassiterite solid solution can be computed from the free energy isotherms via common tangent analysis. The phase relations derived from the different methods are shown in Figure 8 together with the experimental data (Naidu and Virkar, 1998; Park et al., 1975). It is shown that the addition of the $-TS_{vib}$ term significantly stabilizes the disordered phase, causing a shift of the solvus line to lower temperatures by about 250 K. The solvus line calculated based on Monte Carlo simulations shows a critical temperature of 1800 K, which agrees well with the experimental data, 1703±5 K reported by Park et al. (1975) and 1689 K reported by Naidu and Virkar (1998).

5. DISCUSSION

The results obtained with the Monte Carlo method differ noticeably from those obtained via a direct calculation of the partition function. First of all, the comparison of Figures 3a and 3b shows that the enthalpy of the disordered phase in the Monte Carlo model decreases more rapidly. This is the result of SRO, which appears to be more important in the simulations involving a realistically large supercell. The stabilizing effect of SRO seems to be the main cause of the smaller value of the critical temperature predicted with the Monte Carlo simulations. In the disordered limit the enthalpies of mixing calculated with the both methods are similar. Secondly, the low-temperature isotherms in Figures 5b and 5c are strikingly different. This difference can be easily explained. It is important to note that direct calculations apply to a much smaller supercell, in which phase separation typically cannot occur. Indeed, the phase separation implies the contribution of an interface energy. As the formation of such an interface in a small cell is much more unfavorable than in a large cell, the energy of such a cell appears to be much higher than that of a mixture of two phases. Consequently, configurations with the occurrence of such interfaces contribute very little to the total free energy and the entropy. On the other hand, in Monte Carlo simulations, where a much larger supercell is employed, the phase separation occurs. In supercells with approximately intermediate composition the interface is parallel to (100) or (010) (Fig. 6b). These are the same planes across which the compositional fluctuation occurs in the ordered layered structures. This shows that the same interatomic interactions are responsible for both the ordering and the phase separation effects. A phase separated structure can be viewed as an ordered structure composed of layers of infinitely large thickness.

The free energy of a system with a composition falling within a miscibility gap is necessarily a combination of the free energies of the two phases. Ideally, this combination should be represented by a straight line connecting the properties of the two phases. Such straight lines are indeed observed in the Figures 3b, 4c, 5c, however, they occur within a rather narrow intervals at intermediate compositions. The common tangent analysis predicts the phase separation over much wider composition ranges. Small inflections in the isotherms within the miscibility gap are related to changes in the shape of the interface boundary. At intermediate compositions the interface (i.e. the surface which separates phases (slabs) with different compositions) is represented by two parallel planes (Fig. 6b), while at more diluted compositions the interface is a closed curved surface. A similar observations were made by Vinograd and Winkler (2010) when modelling the system NaCl-KCl. Indeed, when the amount of the solute phase is small, there are not enough atoms to make a continuous slab throughout the supercell. As the amount of the second phase increases, the interface area grows until a slab is formed, and further becomes constant. Transitions between these regimes are marked with breaks in the isotherms. It is important to note that in an ideal case of an infinitely large supercell, the interface energy would not have any influence on the thermodynamic functions. This implies that although a reasonably large supercell was employed in our Monte Carlo simulations, our results still correspond to a constrained equilibrium, because the interface energy still matters. Due to the presence of the interface, the enthalpy of the Monte Carlo simulated two-phase assemblage is about 1 kJ/mol higher than this expected for a mechanical mixture.

590 The metastability that is caused by a formation of an interface or by an inability of a cell
591 to phase separate can be removed by a post-simulation common tangent analysis of the
592 shape of the predicted free energy surface. The phase diagram shows that the Monte
593 Carlo simulations agree quite well with the experimental data, while the direct
594 calculations based on a 2 × 2 × 4 supercell considerably overestimate the size of the
595 miscibility gap. The latter is certainly related to the underestimation of the
596 configurational entropy of the disordered phase. The method of Becker at al. (2000)
597 improves the result significantly by decreasing the solvus temperature by 100-200 K.
598 However, the solvus predicted with the direct method still occurs about 100-200 K higher
599 relative to the Monte Carlo result. This effect is likely caused by an underestimation of
600 the relative importance of high-energy configurations within a small cell. Consequently,
601 SRO effects develop to a lesser extent than in a larger cell leading to an overestimation of
602 the free energy of the disordered phase.
603

604 **6. IMPLICATIONS**

605 Currently, two groups of methods offer feasible strategies for the calculation of
606 thermodynamic mixing properties of solid solutions, the direct methods, and the cluster
607 expansion based Monte Carlo methods. The first group of methods is attractive due to the
608 very straightforward computational algorithm, i.e. the direct evaluation of the partition
609 function, and due to a similarly straightforward possibility of evaluation of functions
610 other than the enthalpy and the Gibbs free energy. It appears, however, that direct
611 computation could be performed for rather small supercells only. It also appears that a 2
612 × 2 × 4 supercell (32 exchangeable atoms) is still too small to model correctly the

613 configurational statistics. The correction procedure proposed by Becker et al. (2000) can
614 significantly improve the description of the disordered phase. Monte Carlo simulations
615 provide an alternative indirect approach to the evaluation of the Gibbs free energy, and
616 since a much bigger supercell can be involved in the calculation, the configurational
617 statistics can be treated more accurately. The present study compared the free energies in
618 the rutile-cassiterite system computed with the direct sampling and with the Monte Carlo
619 methods. The same the cluster expansion model was used in the both approaches. This
620 exercise suggested that the Monte Carlo simulations provide a superior description of the
621 free energy of mixing. Thus, in cases when the enthalpy of mixing cannot be computed
622 directly, and where an expansion (parameterization) of the enthalpy should be employed,
623 Monte Carlo simulations seem to offer the best strategy. We note, however, that even an
624 $8 \times 12 \times 16$ supercell does not allow achieving a fully adequate description of the phase
625 separation. The interface energy still matters and affects the shape of free energy
626 isotherms. A small metastability caused by the presence of the interface can be removed
627 by a post-simulation analysis of the curvature of the free energy surface. Our study also
628 shows that including the effect of excess vibrational entropy is important for bringing the
629 results of simulation in an agreement with experiments. In conclusion, we wish to note
630 that the currently available methods of atomistic simulations already provide means for
631 accurate computation of phase diagrams in oxide systems. The present ability to compute
632 an equilibrium content of a solute component in a mineral at a given temperature and
633 pressure offers the possibility of developing geothermometers and geobarometers fully ab
634 initio.
635

ACKNOWLEDGMENT

We acknowledge National Science Foundation of China (Nos. 41425009 and 41230315) and the financial support from the State Key Laboratory for Mineral Deposits Research of China. We acknowledge the computational support from the Juelich Supercomputing Centre, from the Centre for Scientific Computing at the University of Frankfurt and from the High Performance Computing Center of Nanjing University. X. L. is grateful to the China Scholarship Council for financial support. The authors also wish to thank Prof. J. D. Gale (Curtin University) for the help in developing the force-field model.

REFERENCES

Ahrens, T.J. (1995) Mineral physics & crystallography: a handbook of physical constants. American Geophysical Union Washington, DC.

Allan, N., Blundy, J., Purton, J., Lavrentiev, M.Y., and Wood, B. (2001) Trace element incorporation in minerals and melts. Solid Solutions in Silicate and Oxide Systems. EMU Notes in Mineralogy, 3, 251-302.

Allan, N.L., Barrera, G.D., Lavrentiev, M.Y., Freeman, C.L., Todorov, I.T., and Purton, J.A. (2006) Beyond the point defect limit: Simulation methods for solid solutions and highly disordered systems. Computational Materials Science, 36(1–2), 42-48.

Allan, N.L., Barron, T.H.K., and Bruno, J.A.O. (1996) The zero static internal stress approximation in lattice dynamics, and the calculation of isotope effects on molar volumes. The Journal of Chemical Physics, 105(18), 8300-8303.

657 Asato, M., Hoshino, T., and Masuda-Jindo, K. (2001) First-principles calculations for
658 solid solubility limit of impurities in metals:: many-body interaction effect.
659 Journal of Magnetism and Magnetic Materials, 226–230, Part 1(0), 1051-1052.
660 Baur, W. (1956) Über die Verfeinerung der Kristallstrukturbestimmung einiger Vertreter
661 des Rutiltyps: TiO_2, SnO_2, GeO_2 und MgF_2. Acta Crystallographica, 9(6), 515-
662 520.
663 -. (1961) Atomabstande und Bindungswinkel im Brookit, TiO_2. Acta Crystallographica,
664 14(3), 214-216.
665 Becker, U., Fernandez-Gonzalez, A., Prieto, M., Harrison, R., and Putnis, A. (2000)
666 Direct calculation of thermodynamic properties of the barite/celestite solid
667 solution from molecular principles. Physics and Chemistry of Minerals, 27(4),
668 291-300.
669 Bosenick, A., Dove, M.T., and Geiger, C.A. (2000) Simulation studies on the pyrope-
670 grossular garnet solid solution. Physics and Chemistry of Minerals, 27(6), 398-
671 418.
672 Bosenick, A., Dove, M.T., Myers, E.R., Palin, E.J., Sainz-Diaz, C.I., Guiton, B.S.,
673 Warren, M.C., Craig, M.S., and Redfern, S.A.T. (2001) Computational methods
674 for the study of energies of cation distributions: applications to cation-ordering
675 phase transitions and solid solutions. Mineralogical Magazine, 65(2), 193-219.
676 Carp, O., Huisman, C.L., and Reller, A. (2004) Photoinduced reactivity of titanium
677 dioxide. Progress in Solid State Chemistry, 32(1–2), 33-177.
678 Cherniak, D.J., Manchester, J., and Watson, E.B. (2007) Zr and Hf diffusion in rutile.
679 Earth and Planetary Science Letters, 261(1–2), 267-279.

680 Clark, S.J., Segall, M.D., Pickard, C.J., Hasnip, P.J., Probert, M.I.J., Refson, K., and
681 Payne, M.C. (2005) First principles methods using CASTEP. Zeitschrift für
682 Kristallographie, 220(5-6-2005), 567-570.
683 Connolly, J., and Williams, A. (1983) Density-functional theory applied to phase
684 transformations in transition-metal alloys. Physical Review B, 27(8), 5169.
685 D'Arco, P., Mustapha, S., Ferrabone, M., Noël, Y., De La Pierre, M., and Dovesi, R.
686 (2013) Symmetry and random sampling of symmetry independent configurations
687 for the simulation of disordered solids. Journal of Physics: Condensed Matter,
688 25(35), 355401.
689 de Fontaine, D. (1994) Cluster Approach to Order-Disorder Transformations in Alloys. In
690 E. Henry, and T. David, Eds. Solid State Physics, Volume 47, p. 33-176.
691 Academic Press.
692 de Fontaine, D., Wolverton, C., Ceder, G., and Dreysse, H. (1992) Cluster Expansion of
693 fcc Pd-V Intermetallics. In C.T. Liu, R.W. Cahn, and G. Sauthoff, Eds. Ordered
694 Intermetallics — Physical Metallurgy and Mechanical Behaviour, 213, p. 61-71.
695 Springer Netherlands.
696 Dove, M.T. (1999) Order/disorder phenomena in minerals: ordering phase transitions and
697 solid solutions. NATO ASI Series, Series C Mathematical and Physical Sciences,
698 543, 451-476.
699 Dove, M.T. (2001) Computer simulations of solid solutions. Solid Solutions in Silicate
700 and Oxide Systems. EMU Notes in Mineralogy, 3, 225-249.
701 Dove, M.T., Bosenick, A., Myers, E.R., Warren, M.C., and Redfern, S.A.T. (2000)
702 Modelling in relation to cation ordering. Phase Transitions, 71(3), 205-226.

703 Dove, M.T., Thayaparam, S., Heine, V., and Hammonds, K. (1996) The phenomenon of
704 low AI-Si ordering temperatures in aluminosilicate framework structures.
705 American Mineralogist, 81, 349-362.
706 Ferriss, E.D.A., Ewing, R.C., and Becker, U. (2010) Simulation of thermodynamic
707 mixing properties of actinide-containing zircon solid solutions. American
708 Mineralogist, 95(2-3), 229-241.
709 Finel, A. (1994) The Cluster Variation Method and Some Applications. In P.A. Turchi,
710 and A. Gonis, Eds. Statics and Dynamics of Alloy Phase Transformations, 319, p.
711 495-540. Springer US.
712 Fujishima, A., and Honda, K. (1972) Electrochemical photolysis of water at a
713 semiconductor electrode. Nature(238), 37-8.
714 Gale, J.D. (1997) GULP: A computer program for the symmetry-adapted simulation of
715 solids. J. Chem. Soc., Faraday Trans., 93(4), 629-637.
716 Gale, J.D. (2005) GULP: Capabilities and prospects. Zeitschrift für Kristallographie -
717 Crystalline Materials, 220(5-6-2005), 552-554.
718 Gale, J.D., and Rohl, A.L. (2003) The general utility lattice program (GULP). Molecular
719 Simulation, 29(5), 291-341.
720 Ganguly, J. (2001) Thermodynamic modelling of solid solutions. Solid Solutions in
721 Silicate and Oxide Systems. EMU Notes in Mineralogy, 3, 37-70.
722 Garcia, D., and Speidel, D. (1972) Reexamination of the System TiO_2-SnO_2. Journal of
723 the American Ceramic Society, 55(6), 322-322.
724 Glynn, P. (2000) Solid-Solution Solubilities and Thermodynamics: Sulfates, Carbonates
725 and Halides. Reviews in Mineralogy & Geochemistry, 40(1), 481-511.

726 Grau-Crespo, R., de Leeuw, N.H., and Catlow, C.R.A. (2004) Distribution of Cations in
727 FeSbO4: A Computer Modeling Study. Chemistry of Materials, 16(10), 1954-
728 1960.
729 Grau-Crespo, R., Hamad, S., Catlow, C.R.A., and Leeuw, N.H.d. (2007) Symmetry-
730 adapted configurational modelling of fractional site occupancy in solids. Journal
731 of Physics: Condensed Matter, 19(25), 256201.
732 Horn, M., Schwerdtfeger, C.F., and Meagher, E.P. (1972) Refinement of the structure of
733 anatase at several temperatures. Zeitschrift für Kristallographie - Crystalline
734 Materials, 136(1-6), 273-281.
735 Hoshino, T., Schweika, W., Zeller, R., and Dederichs, P. (1993) Impurity-impurity
736 interactions in Cu, Ni, Ag, and Pd. Physical Review B, 47(9), 5106.
737 Hoshino, T., Zeller, R., and Dederichs, P.H. (1996) Local-density-functional calculations
738 for defect interactions in Al. Physical Review B, 53(14), 8971-8974.
739 Jiang, C. (2008) First-principles study of $Co_3(Al,W)$ alloys using special quasi-random
740 structures. Scripta Materialia, 59(10), 1075-1078.
741 Jung, D.Y., Vinograd, V.L., Fabrichnaya, O.B., Oganov, A.R., Schmidt, M.W., and
742 Winkler, B. (2010) Thermodynamics of mixing in $MgSiO_3$–Al_2O_3 perovskite and
743 ilmenite from ab initio calculations. Earth and Planetary Science Letters, 295(3-
744 4), 477-486.
745 Kulik, D.A., Vinograd, V.L., Paulsen, N., and Winkler, B. (2010) $(Ca,Sr)CO_3$ aqueous–
746 solid solution systems: From atomistic simulations to thermodynamic modelling.
747 Physics and Chemistry of the Earth, 35(6–8), 217-232.

748 Laks, D.B., Ferreira, L.G., Froyen, S., and Zunger, A. (1992) Efficient cluster expansion
749 for substitutional systems. Physical Review B, 46(19), 12587-12605.
750 Liu, X., Lu, X., Liu, X., and Zhou, H. (2015) Atomistic simulation on mixing
751 thermodynamics of calcite-smithsonite solid solutions. American Mineralogist,
752 100(1), 172-180.
753 Metropolis, N., Rosenbluth, A.W., Rosenbluth, M.N., Teller, A.H., and Teller, E. (1953)
754 Equation of State Calculations by Fast Computing Machines. The Journal of
755 Chemical Physics, 21(6), 1087-1092.
756 Myers, E.R. (1998) A statistical-mechanics model of ordering in aluminosilicate solid
757 solutions. Physics and chemistry of minerals, 25(6), 465-468.
758 Naidu, H.P., and Virkar, A.V. (1998) Low-Temperature TiO_2-SnO_2 Phase Diagram
759 Using the Molten-Salt Method. Journal of the American Ceramic Society, 81(8),
760 2176-2180.
761 Onsager, L. (1944) Crystal Statistics. I. A Two-Dimensional Model with an Order-
762 Disorder Transition. Physical Review, 65(3-4), 117-149.
763 Padurow, N. (1956) Miscibility in the System Rutile-cassiterite. Naturwissenschaften,
764 43(17), 395-396.
765 Palin, E.J., Dove, M.T., Redfern, S.A.T., Bosenick, A., Sainz-Diaz, C.I., and Warren,
766 M.C. (2001) Computational study of tetrahedral Al–Si ordering in muscovite.
767 Physics and Chemistry of Minerals, 28(8), 534-544.
768 Park, M., Mitchell, T.E., and Heuer, A.H. (1975) Subsolidus Equilibria in the TiO_2-SnO_2
769 System. Journal of the American Ceramic Society, 58(1-2), 43-47.

Prieto, M., Fernandez-Gonzalez, A., Becker, U., and Putnis, A. (2000) Computing Lippmann diagrams from direct calculation of mixing properties of solid solutions: Application to the barite-celestite system. Aquatic Geochemistry, 6(2), 133-146.

Purton, J.A., Allan, N.L., Lavrentiev, M.Y., Todorov, I.T., and Freeman, C.L. (2006) Computer simulation of mineral solid solutions. Chemical Geology, 225(3–4), 176-188.

Reich, M., and Becker, U. (2006) First-principles calculations of the thermodynamic mixing properties of arsenic incorporation into pyrite and marcasite. Chemical Geology, 225(3-4), 278-290.

Renock, D., and Becker, U. (2011) A first principles study of coupled substitution in galena. Ore Geology Reviews, 42(1), 71-83.

Ringwood, A.E., Kesson, S.E., Ware, N.G., Hibberson, W., and Major, A. (1979a) Immobilisation of high level nuclear reactor wastes in SYNROC. Nature, 278(5701), 219-223.

Ringwood, A.E., Kesson, S.E., Ware, N.G., Hibberson, W.O., and Major, A. (1979b) The SYNROC process: A geochemical approach to nuclear waste immobilization. Geochemical Journal, 13(4), 141-165.

Sanchez, J.M., and de Fontaine, D. (1978) The fcc Ising model in the cluster variation approximation. Physical Review B, 17(7), 2926-2936.

Sanchez, J.M., Ducastelle, F., and Gratias, D. (1984) Generalized cluster description of multicomponent systems. Physica A: Statistical Mechanics and its Applications, 128(1), 334-350.

Segall, M., Lindan, P.J., Probert, M.a., Pickard, C., Hasnip, P., Clark, S., and Payne, M. (2002) First-principles simulation: ideas, illustrations and the CASTEP code. Journal of Physics: Condensed Matter, 14(11), 2717.

Sikora, R. (2005) Ab initio study of phonons in the rutile structure of TiO_2. Journal of Physics and Chemistry of Solids, 66(6), 1069-1073.

Sluiter, M., and Kawazoe, Y. (2003) Cluster expansion method for adsorption: Application to hydrogen chemisorption on graphene. Physical Review B, 68(8).

Swope, R.J., Smyth, J.R., and Larson, A.C. (1995) H in rutile-type compounds: I. Single-crystal neutron and X-ray diffraction study of H in rutile. American Mineralogist, 80(5), 448-453.

Todorov, I.T., Allan, N.L., Lavrentiev, M.Y., Freeman, C.L., Mohn, C.E., and Purton, J.A. (2004) Simulation of mineral solid solutions at zero and high pressure using lattice statics, lattice dynamics and Monte Carlo methods. Journal of Physics: Condensed Matter, 16(27), S2751.

Urusov, V.S., Khisina, N.R., and Christy, A.G. (1996) Quasi-equilibrium behaviour of TiO_2-SnO_2 solid solutions at high pressures and temperatures; the influence of non-hydrostaticity. European Journal of Mineralogy, 8(4), 791-804.

van de Walle, A., and Asta, M. (2002) Self-driven lattice-model Monte Carlo simulations of alloy thermodynamic properties and phase diagrams. Modelling and Simulation in Materials Science and Engineering, 10(5), 521.

van de Walle, A., and Ceder, G. (2002a) Automating first-principles phase diagram calculations. Journal of Phase Equilibria, 23(4), 348-359.

-. (2002b) The effect of lattice vibrations on substitutional alloy thermodynamics. Reviews of Modern Physics, 74(1), 11-45.

Vinograd, V., Burton, B., Gale, J., Allan, N., and Winkler, B. (2007) Activity–composition relations in the system $CaCO_3$–$MgCO_3$ predicted from static structure energy calculations and Monte Carlo simulations. Geochimica et Cosmochimica Acta, 71(4), 974-983.

Vinograd, V., Sluiter, M., and Winkler, B. (2009) Subsolidus phase relations in the $CaCO_3 - MgCO_3$ system predicted from the excess enthalpies of supercell structures with single and double defects. Physical Review B, 79(10).

Vinograd, V., and Winkler, B. (2010) An Efficient Cluster Expansion Method for Binary Solid Solutions: Application to the Halite-Silvite, NaCl-KCl, System. Reviews in Mineralogy & Geochemistry, 71(1), 413-436.

Vinograd, V., Winkler, B., Putnis, A., Gale, J., and Sluiter, M. (2006) Static lattice energy calculations of mixing and ordering enthalpy in binary carbonate solid solutions. Chemical Geology, 225(3-4), 304-313.

Vinograd, V.L., Brandt, F., Rozov, K., Klinkenberg, M., Refson, K., Winkler, B., and Bosbach, D. (2013) Solid–aqueous equilibrium in the $BaSO_4$–$RaSO_4$–H_2O system: First-principles calculations and a thermodynamic assessment. Geochimica et Cosmochimica Acta, 122(0), 398-417.

Warren, M.C., Dove, M.T., Myers, E.R., Bosenick, A., Palin, E.J., Sainz-Diaz, C.I., Guiton, B.S., and Redfern, S.A.T. (2001) Monte Carlo methods for the study of cation ordering in minerals. Mineralogical Magazine, 65(2), 221-248.

837 Watson, E.B., Wark, D.A., and Thomas, J.B. (2006) Crystallization thermometers for
838 zircon and rutile. Contributions to Mineralogy and Petrology, 151(4), 413-433.
839 Wei, S.H., Ferreira, L.G., Bernard, J.E., and Zunger, A. (1990) Electronic properties of
840 random alloys: Special quasirandom structures. Physical Review B, 42(15), 9622-
841 9649.
842 Will, T.M. (1998) Thermodynamics of solid solutions. Phase Equilibria in Metamorphic
843 Rocks, 71, p. 9-85. Springer Berlin Heidelberg.
844 Wolverton, C., Asta, M., Dreyssé, H., and de Fontaine, D. (1991) Effective cluster
845 interactions from cluster-variation formalism. II. Physical Review B, 44(10),
846 4914-4924.
847 Wu, Z., and Cohen, R.E. (2006) More accurate generalized gradient approximation for
848 solids. Physical Review B, 73(23), 235116.
849 Xu, H., and Wang, Y. (2000) Crystallization sequence and microstructure evolution of
850 Synroc samples crystallized from $CaZrTi_2O_7$ melts. Journal of Nuclear Materials,
851 279(1), 100-106.
852 Zack, T., Moraes, R., and Kronz, A. (2004a) Temperature dependence of Zr in rutile:
853 empirical calibration of a rutile thermometer. Contributions to Mineralogy and
854 Petrology, 148(4), 471-488.
855 Zack, T., von Eynatten, H., and Kronz, A. (2004b) Rutile geochemistry and its potential
856 use in quantitative provenance studies. Sedimentary Geology, 171(1–4), 37-58.
857 Zhang, Y., Hart, K.P., Bourcier, W.L., Day, R.A., Colella, M., Thomas, B., Aly, Z., and
858 Jostsons, A. (2001) Kinetics of uranium release from Synroc phases. Journal of
859 Nuclear Materials, 289(3), 254-262.

860 Zunger, A., Wei, S.H., Ferreira, L.G., and Bernard, J.E. (1990) Special quasirandom
861 structures. Physical Review Letters, 65(3), 353-356.

862

863

864

865

866

867

Figure 1. Enthalpy of mixing in the rutile-cassitertite system at an infinitely high temperature. The solid line is a subregular (two-parameter) fit to the excess energies of the structures with single defects.

Figure 2. Pairwise interactions computed from the excess enthalpies of the structures with single and paired defects.

Figure 3. (**a**) Isotherms of enthalpy of mixing in the rutile-cassitertite solid solution computed with the direct method (DM) using a 2 × 2 × 4 supercell. The enthalpies of the individual configurations are computed with Eq. 7. (**b**) Isotherms of the enthalpy of mixing computed with Monte Carlo simulations using an 8 × 12 × 16 supercell. Isotherms are 100 K apart.

Figure 4. Isotherms of Gibbs free energy of mixing in the rutile-cassitertite solid solution, (**a**) computed with the direct method using a 2 × 2 × 4 supercell, (**b**) computed with the direct method with the correction after Becker et al. (2000) using a 2 × 2 × 4 supercell, (**c**) computed with Monte Carlo simulations using an 8 × 12 × 16 supercell. Isotherms are 100 K apart.

Figure 5. Isotherms of the configurational entropy of mixing in the rutile-cassitertite solid solution, (**a**) computed with the direct method (DM) using a 2 × 2 × 4 supercell, (**b**) computed with the direct method with the correction after Becker et al. (2000) using a 2 ×

892 2 × 4 supercell, (**c**) computed with Monte Carlo simulations using an 8 × 12 × 16
893 supercell. Isotherms are 100 K apart.
894
895 **Figure 6.** Phase separation occurred during the Monte Carlo simulation runs for different
896 compositions simulated at 600 K, (**a**) x_{Sn}=3/32 and (**b**) x_{Sn}=16/32. Blue and brown balls
897 represent Ti and Sn atoms, respectively. O atoms are not shown.
898
899 **Figure 7.** Excess vibrational entropy computed from the force-field model. The vertical
900 bars reflect the variation of the values within the temperature interval of 1473-1773 K.
901
902 **Figure 8.** The subsolidus phase diagram of the rutile-cassitertite system. Dash lines and
903 solid lines are the results of the simulations before and after vibrational entropy
904 correction, respectively. Squares and the black curve denote the experimental data.
905
906
907
908
909
910

Table 1. Parameters of the interatomic potentials for rutile and cassiterite.

Buckingham potential	A, eV	ρ, Å	C, eV *Å^6	cutoff, Å
Ti core - O shell	84045.732	0.159447	0.000	12.0
Sn core - O shell	376724.00	0.148615	0.000	12.0
O shell - O shell	1294.9157	0.317190	27.961	12.0
Charge and Spring potential	**core**	**shell**	K_2, eV/Å^2	
Ti	2.239195			
Sn	2.239195			
O	0.517015	-1.636611	25.830181	

Table 2. Structural and elastic properties of TiO_2 and SnO_2: experimental data and results of the force-field calculation.

	TiO_2		SnO_2	
	experiment[a]	calculation	experiment[b]	calculation
a, Å	4.592	4.569	4.737	4.755
c, Å	2.957	2.994	3.185	3.160
V, Å^3	62.366	62.497	71.468	71.450
C_{11}, GPa	269.0	306.8	261.7	285.9
C_{12}, GPa	177.0	175.2	177.2	199.8
C_{13}, GPa	146.0	147.4	155.5	151.7
C_{33}, GPa	480.0	462.5	449.6	427.7
C_{44}, GPa	124.0	125.1	103.1	103.4
C_{66}, GPa	192.0	179.1	207.4	198.0

a: Structure properties are from Swope et al. (1995) and elastic properties are from Ahrens (1995).
b: Structure properties are from Baur (1956) and elastic properties are from Ahrens (1995)..

Table 3. Excess enthalpies of double defects and the J values.

n	*Distance*, Å	D_n	ΔH, eV per supercell		J values, kJ/mol	
			Ti-Ti defects in SnO_2	Sn-Sn defects in TiO_2	J_{Ti}	J_{Sn}
1	2.959	1	0.6816	0.7286	7.4613	9.5523
2	3.569	1	0.7616	0.7855	1.9713	1.8335
3	4.593	2	0.6964	0.7122	4.5218	4.0621
4	5.464	2	0.7428	0.7496	2.7175	1.8237
5	5.500	1	0.7681	0.7854	1.9809	1.2063
6	5.918	2	0.8064	0.9465	-6.7814	-1.2445
7	6.495	4	0.8003	0.8377	-0.7663	-0.4751
8	7.138	4	0.7801	0.8247	-0.4527	0.0121
9	7.491	4	0.7545	0.7508	1.3298	0.6296
10	8.787	8	0.7790	0.7938	0.1463	0.0193

922

Figure 1

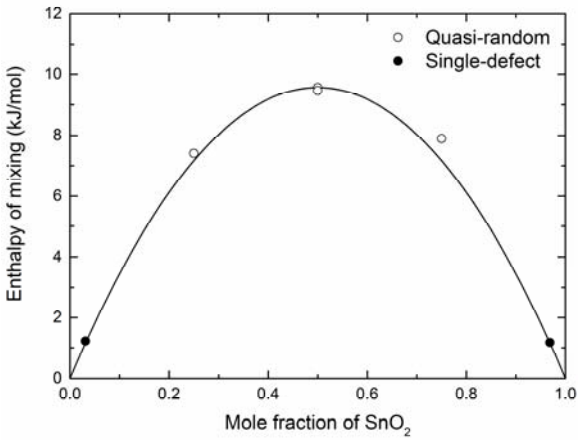

923

924

Figure 2

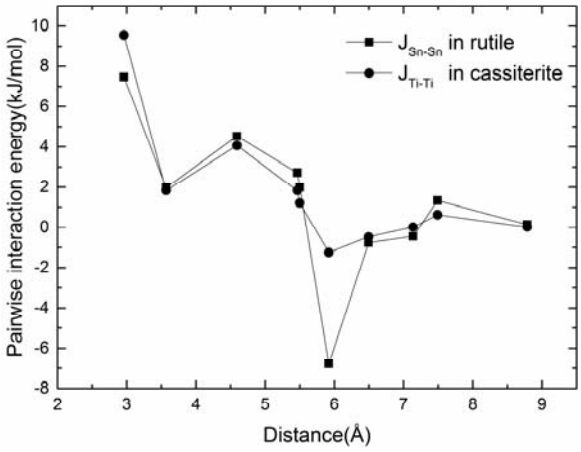

925

926

Figure 3a

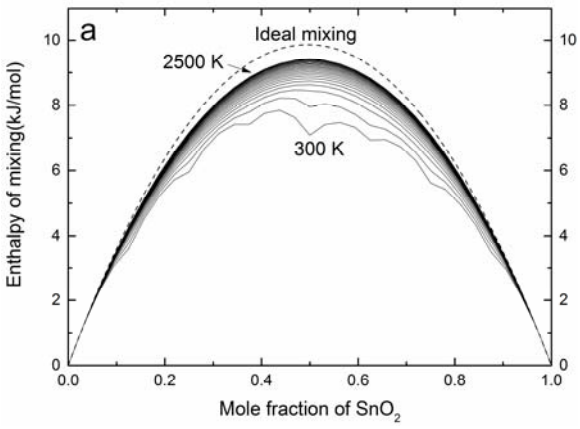

927

Figure 3b

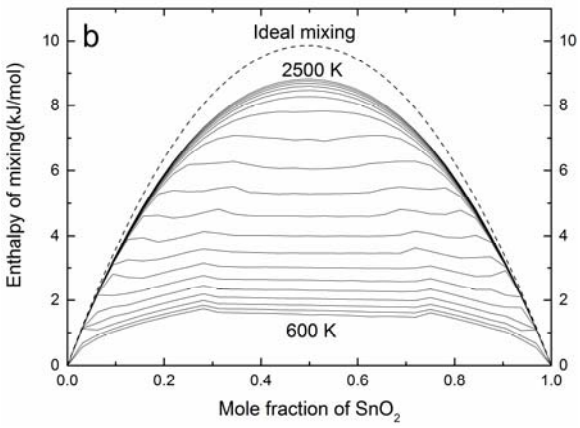

928

929

Figure 4a

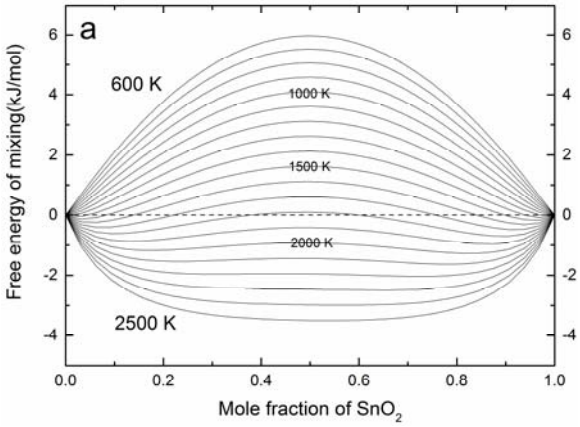

930

931

Figure 4b

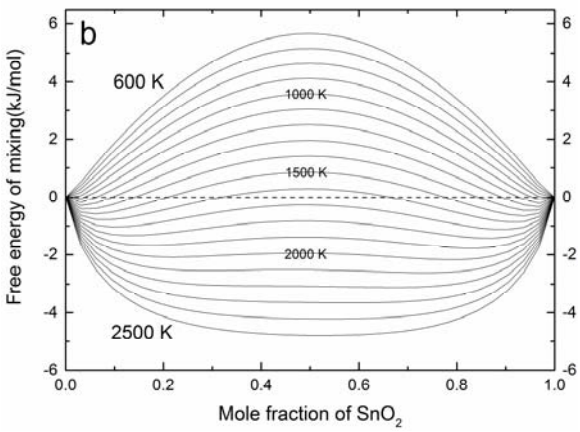

932

933

934

Figure 4c

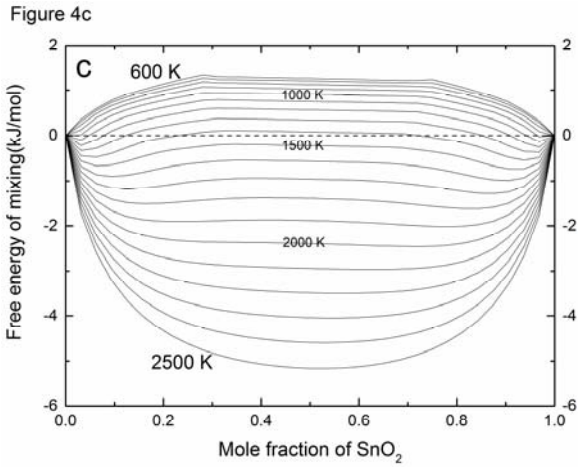

935

936

Figure 5a

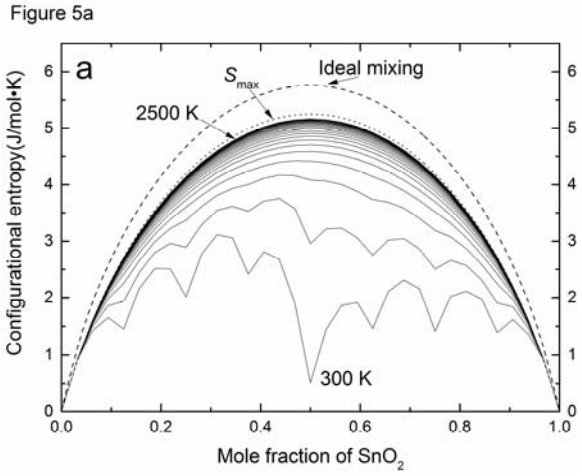

937

938

Figure 5b

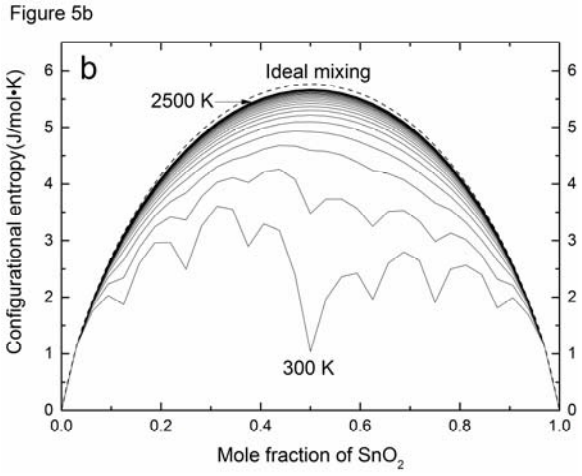

939

Figure 5c

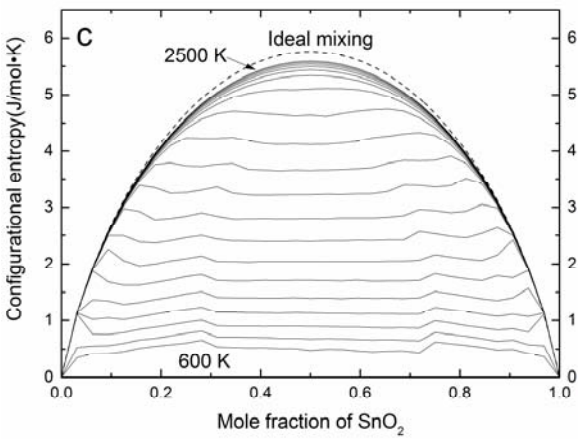

940

941

Figure 6

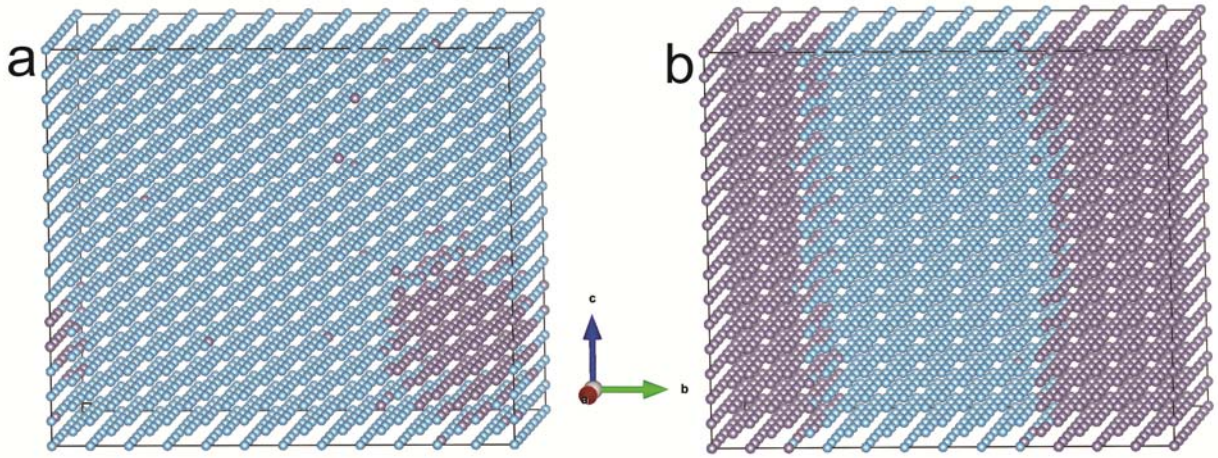

942

943

Figure 7

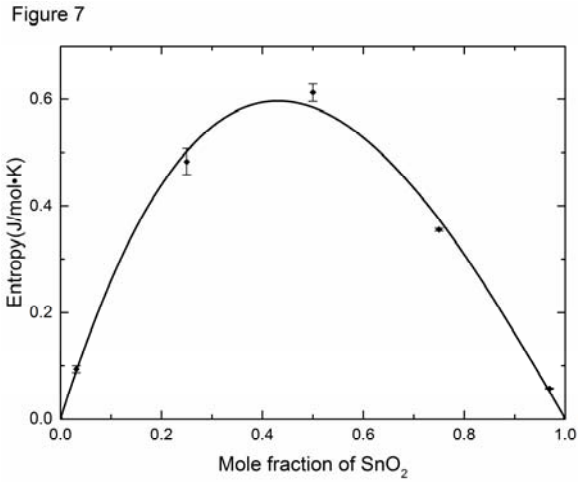

944

945

Figure 8

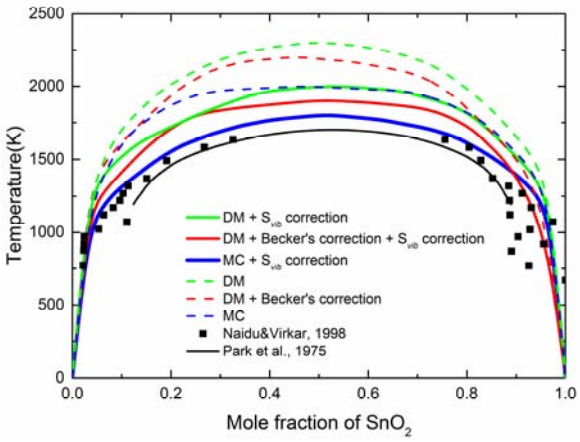

946

947

This is a preprint, the final version is subject to change, of the American Mineralogist (MSA)
Cite as Authors (Year) Title. American Mineralogist, in press.
(DOI will not work until issue is live.) DOI: http://dx.doi.org/10.2138/am-2016-5490

Figure 1

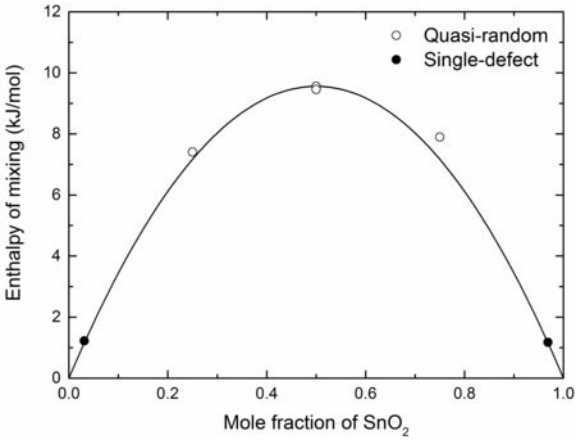

This is a preprint, the final version is subject to change, of the American Mineralogist (MSA)
Cite as Authors (Year) Title. American Mineralogist, in press.
(DOI will not work until issue is live.) DOI: http://dx.doi.org/10.2138/am-2016-5490

Figure 2

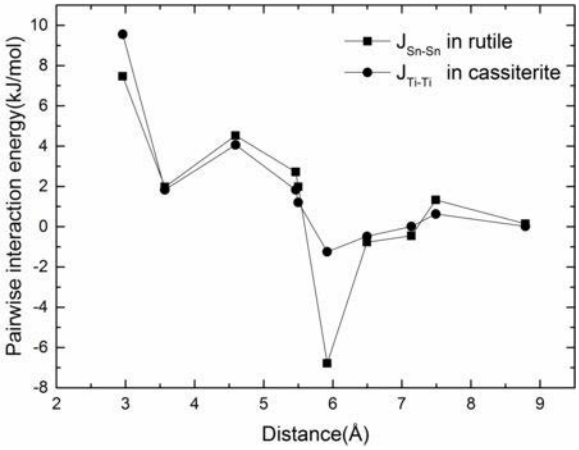

This is a preprint, the final version is subject to change, of the American Mineralogist (MSA)
Cite as Authors (Year) Title. American Mineralogist, in press.
(DOI will not work until issue is live.) DOI: http://dx.doi.org/10.2138/am-2016-5490

Figure 3a

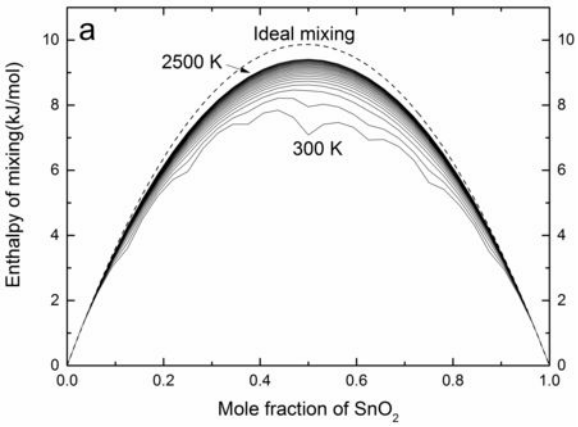

This is a preprint, the final version is subject to change, of the American Mineralogist (MSA)
Cite as Authors (Year) Title. American Mineralogist, in press.
(DOI will not work until issue is live.) DOI: http://dx.doi.org/10.2138/am-2016-5490

Figure 3b

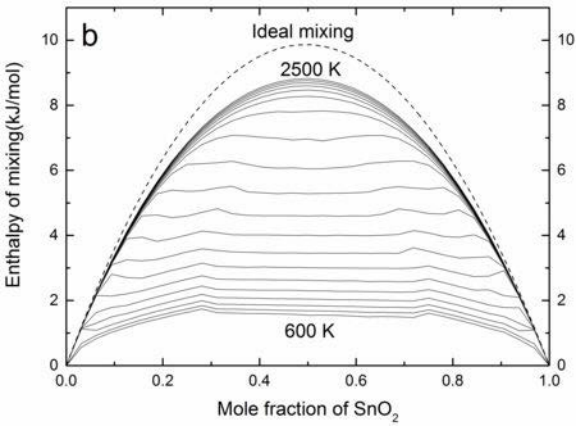

This is a preprint, the final version is subject to change, of the American Mineralogist (MSA)
Cite as Authors (Year) Title. American Mineralogist, in press.
(DOI will not work until issue is live.) DOI: http://dx.doi.org/10.2138/am-2016-5490

Figure 4a

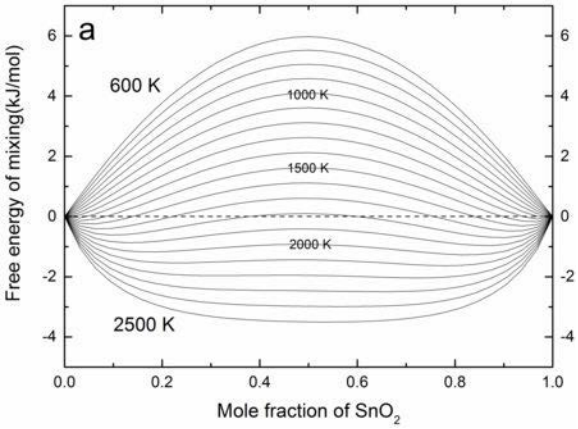

This is a preprint, the final version is subject to change, of the American Mineralogist (MSA)
Cite as Authors (Year) Title. American Mineralogist, in press.
(DOI will not work until issue is live.) DOI: http://dx.doi.org/10.2138/am-2016-5490

Figure 4b

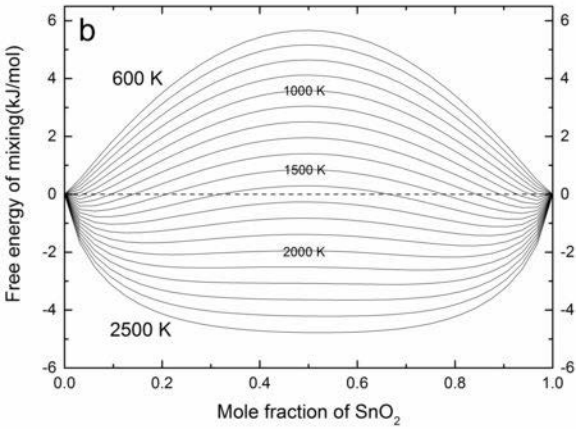

This is a preprint, the final version is subject to change, of the American Mineralogist (MSA)
Cite as Authors (Year) Title. American Mineralogist, in press.
(DOI will not work until issue is live.) DOI: http://dx.doi.org/10.2138/am-2016-5490

Figure 4c

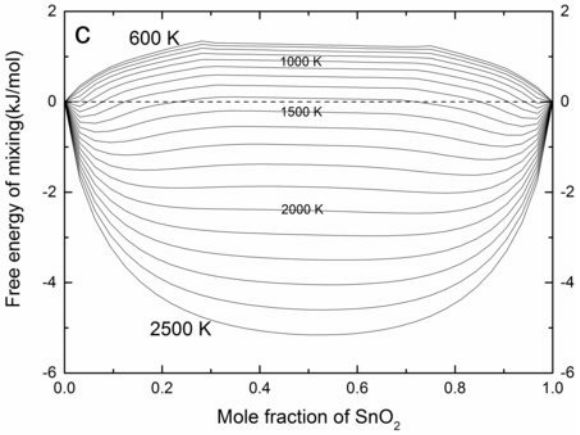

This is a preprint, the final version is subject to change, of the American Mineralogist (MSA)
Cite as Authors (Year) Title. American Mineralogist, in press.
(DOI will not work until issue is live.) DOI: http://dx.doi.org/10.2138/am-2016-5490

Figure 5a

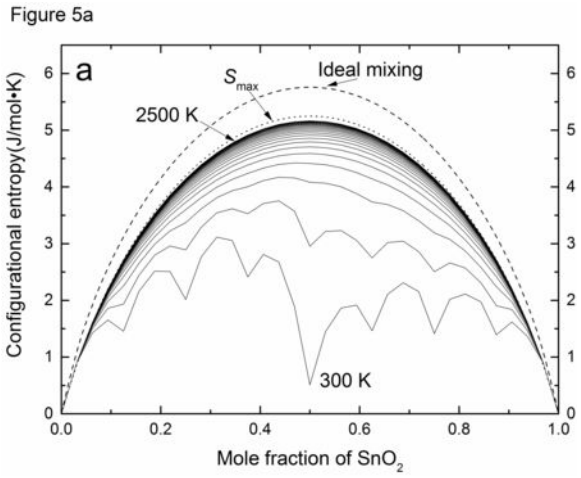

This is a preprint, the final version is subject to change, of the American Mineralogist (MSA)
Cite as Authors (Year) Title. American Mineralogist, in press.
(DOI will not work until issue is live.) DOI: http://dx.doi.org/10.2138/am-2016-5490

Figure 5b

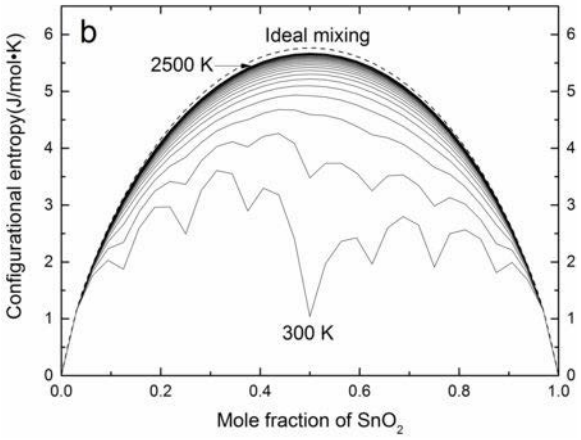

This is a preprint, the final version is subject to change, of the American Mineralogist (MSA)
Cite as Authors (Year) Title. American Mineralogist, in press.
(DOI will not work until issue is live.) DOI: http://dx.doi.org/10.2138/am-2016-5490

Figure 5c

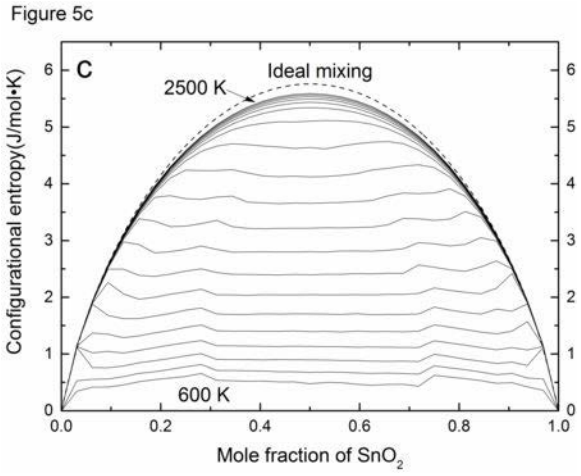

This is a preprint, the final version is subject to change, of the American Mineralogist (MSA)
Cite as Authors (Year) Title. American Mineralogist, in press.
(DOI will not work until issue is live.) DOI: http://dx.doi.org/10.2138/am-2016-5490

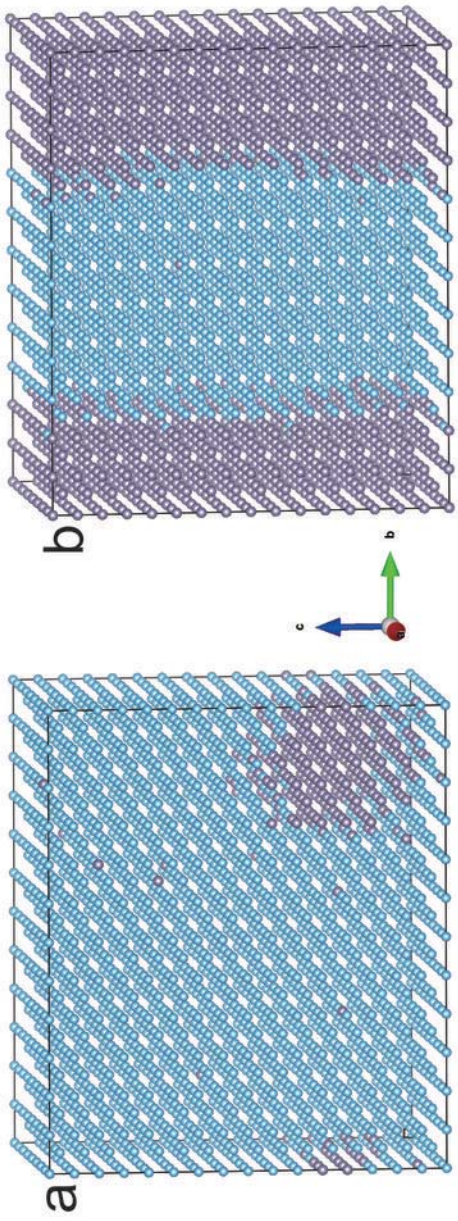

Figure 6

This is a preprint, the final version is subject to change, of the American Mineralogist (MSA)
Cite as Authors (Year) Title. American Mineralogist, in press.
(DOI will not work until issue is live.) DOI: http://dx.doi.org/10.2138/am-2016-5490

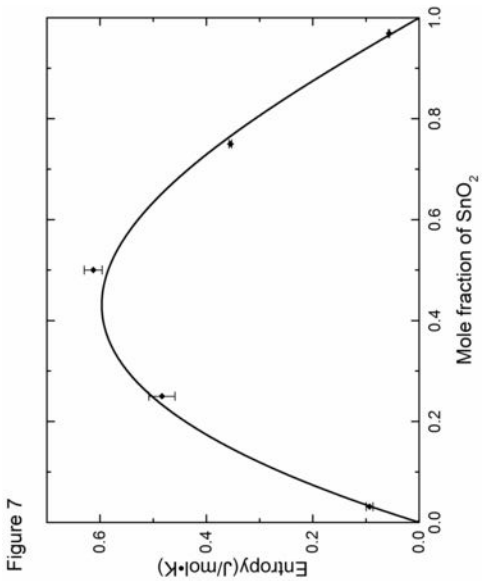

Figure 7

This is a preprint, the final version is subject to change, of the American Mineralogist (MSA)
Cite as Authors (Year) Title. American Mineralogist, in press.
(DOI will not work until issue is live.) DOI: http://dx.doi.org/10.2138/am-2016-5490

Figure 8